Proceedings of the 17th World Congress
The International Federation of Automatic Control
Seoul, Korea, July 6-11, 2008

Defect Classification Using Bayesian Approach for Tape Substrate Inspection System

YoungJun Roh*, CheolWoo Kim, ChangOok Jung, and Daehwa Jeong.

** Production Research Institute, LG Electronics.*
Korea (Tel: 82-31-660-7860; e-mail : behero71@lge.com,)

Abstract: The inspection of ultra-fine pitch patterned tape substrate (TS) requires high resolution optics. In the process of picking out defects at the level of the critical dimension through image processing, however, trivial blemishes formed by dust or micro particles may be detected simultaneously. This leads to unnecessary work on the part of operators reviewing and verifying the additional detected points. To maximize the efficiency of the inspection process, we need to identify and classify the defect candidates whether it is a real pattern defect or simply a trivial blemish by dust. In this article, we propose a Bayesian approach to classify the defective images based on the measures of the image features. The features of the defective region in terms of shape and brightness are obtained from a series of proper image analysis with FFT. Based on the data collected from experiments, we devised a statistic model for classification.

1. INTRODUCTION

Tape substrate (TS) products, as illustrated in Fig. 1 (a), such as tape carrier package (TCP) and chip on film (COF) comprise of fine electric circuit pattern printed on a very thin and flexible polyimide (PI) film. Due to their compactness and high density, they are used for packaging display drive ICs in flat panel display products such as PDP and LCD (Thompson *et al*., 1999). In accordance with the advancement in electronic packaging technologies, TS products are nowadays becoming increasingly fine; in critical regions of the circuit pattern, the dimension is less than 25μm pitch with 8μm circuit width. Like printed circuit boards (PCB), TS is produced through a series of etching processes, and defects in the pattern such as open/short and nick and protrusion that can cause malfunctions in final products (Fig. 1. (b)). When a product's dimension goes down to micrometer scale as in our application, foreign particles in the order of micrometers within the substrate materials and dust adhesion during the production process can deter reliable defect detection. Due to the lack of intelligence in the inspection process, these particles tend to be detected as defect candidates. For this reason, in most high resolution inspection for products such as LCD, PDP and lead frame, an additional review and verification process by operators is required added after the automated inspection (Moganti, 1996, Lim *et al*., 2001). To reduce the effort in verifying these trivial points, a video defect classification (VDC) approach has been investigated by researchers, where a high magnified colour image is utilized for automatic classification with more clues (Lim *et al*., 2001). In the subsequent section, we introduce the architecture of a network structured inspection system, where a server and client systems are used for review and verification. And we briefly describe defect detection algorithms based on graph matching and design rule approach.

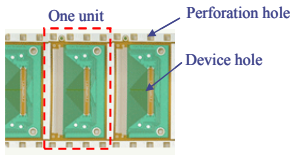

(a) Chip on film (COF)

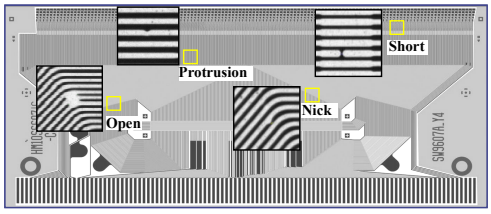

(b) Pattern defects

Fig. 1. Chip on film and the defect types

To minimize the number of points to be reviewed by the operators and make the process more efficient, we propose an image feature based classification method in the subsequent sections. In chapter 3, the image features and the processing methods that describe whether a defective point is a dust or a real defect are discussed. To discriminate real defects and dust among the defect candidates, we propose two indices that indicate the likelihood of pattern defect in the view point of shape and brightness. By utilizing the measures on the image features, Bayesian approach is implemented in this work for the classification (Bayes, 1763). The statistic

models for Bayesian inference are obtained from the experiments on a number of images. The performance of the proposed classifier is tested on another image set and the results are discussed in chapter 4.

2. TAPE SUBSTRATE INSPECTION

2.1 TS Inspection System.

Fig. 2 shows a network structured TS inspection system, which consists of TS visual inspection machines, punching machines, a server, and client verification systems. In the inspection machines, tape products are inspected by using a series of line cameras while they pass through the inspection zone by a reel-to-reel transfer unit. We utilized four line cameras with different illumination to detect not only pattern defects such as open, short, nick and protrusion but also exterior blemishes like scratches or discoloration on the product surface. The optical resolution for detecting pattern and surface defects is 1.9um and 3.5um, respectively, which gives rise to huge inspection images exceeding 600MB per unit. A high computation power processing module equipped with 128 DSPs makes it possible to process the massive information real time by parallel processing. The output defective image clip, made up of small sized images (128x128 pixels) encompassing the detected points, called defect candidates, are transferred to a server system in run time (Roh *et al*., 2005).

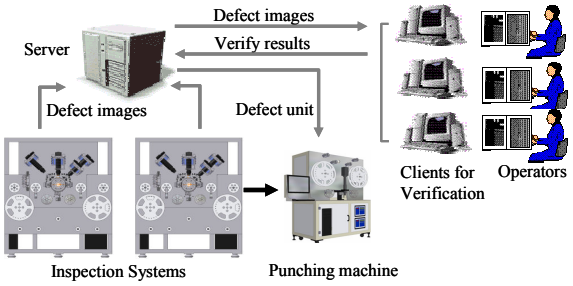

Fig. 2. A network structured inspection system.

Since not only actual defects but also numerous trivial blemishes due to dust or foreign substances may be included among the defect candidates, they need to be checked for their authenticity. For this purpose, operators review the candidate images and verify them at the client desks, and the judged results are sent back to the server system. The fact that the verification is conducted on a network without interfering the inspection process itself allows the inspection and verification processes be run in a parallel and efficient way. When the inspection is completed, the reel is transferred to a punching machine along with the operator-judged results from the server. Finally, at the punching machine, units that have been judged as being defective during the verification process are punched and are no longer usable.

2.2 Defect detection.

To inspect the pattern from a captured image, we utilize both the referential and non-referential method. To check for the soundness of the circuit connection, we utilize a graph matching method, where the designed connectivity rules of the circuit are collected from a master image, and then are compared to those in the inspection image. For this purpose, we represent a circuit pattern as a path that links between two or more distinct points, thereafter a pattern l_k is modeled by a set of linked N link points $\mathbf{P}_n$ like as:

$$l_k = \{\mathbf{P}_1, \mathbf{P}_2, ..., \mathbf{P}_N\} \tag{1}$$

Considering that the inspection here is made tile-wisely, a set of link points of a pattern can be defined where a pattern meets the border of the tile.

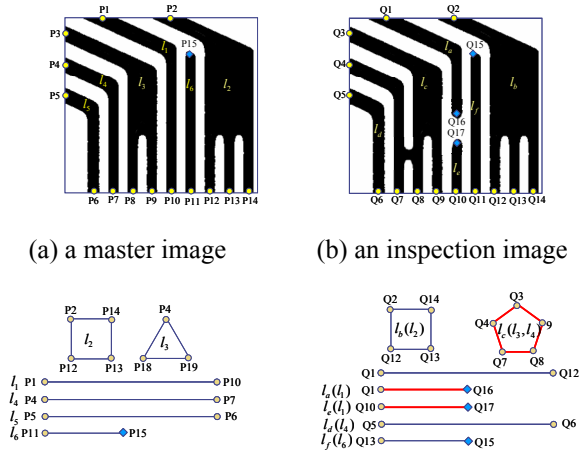

Fig. 3. Graph representation of patterns

Fig. 3 (c) shows an graph model representation of a tile image Fig. 3 (a), where we can intuitively find that 6 lines l_1,l_2,…,l_6 are present with 15 endpoints P_1,P_2,…,P_{15}. The end points on the borders of the tile are defined as link points, and an exceptional case of point P_{15} is called as a terminal point in this work. Graphically, the lines are represented by a line or a polygon according to the number of the endpoints as shown in Fig. 3 (c), where the terminal point is marked as a symbol of diamond. Once the patterns are graphically represented in this manner, a misconnection defects like open and short can be easily detected by checking the number of link points: when an inspected pattern is modeled with a smaller (or a larger) number of link points compared to that of its master pattern, it can be regarded as an open (or a short) defect. Let us investigate a defective image of Fig. 3 (b) as an example, where an open and a short defect are present. The inspection image is modeled with a graph model with six lines l_a,l_b,…,l_f and 17 link points, Q_1,Q_2,…,Q_{17}, which is graphically represented by Fig. 3 (d). When the correspondence of each line is found by a proper searching, and the end points of each graph are compared to the

reference one in Fig. 3. (c), we can find the difference between the graphs. The pattern l_c is composed of five link points, on the other hand, the corresponding pattern l_3 in the master graph has three link points, and therefore it is determined as a short defect. In case of l_a or l_e, they have one link and one terminal point, which is less than two link point of its corresponding pattern l_1, and therefore are decided as open defects. The graph matching method is described in detail in reference (Roh *et al*., 2006). In addition to the critical open or short defects, TS products can have latent defects such as nick and protrusion caused by over and under etching, respectively. Although these defects do not cause any immediate electrical malfunction, they can become a critical open or short defect in future when the TS product is bent during integration. These defects on the pattern's boundary are detected on the inspection image itself, which is called as a non-referential method. Over-etching and under-etching points are determined as defects when more than 1/3 of the designed pattern width ω or spacer σ is intruded, respectively. For defect detection according to this criterion, the dimension of pattern and spacer width is measured by counting pixels along horizontal or vertical direction. Due to the variations in pattern line width among the products, a fixed dimension for reference is not available here. Instead of using a reference dimension, we investigate the pattern width along the lines and detect the singularity point, if any, where a sudden change in pattern width is found as illustrated in Fig. 4.

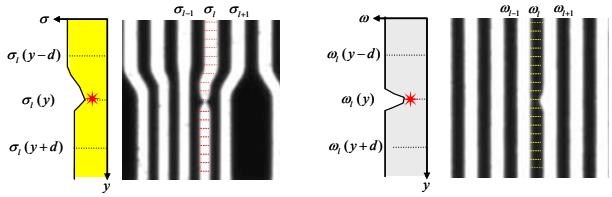

(a) protrusion on spacer (b) nick on pattern

Fig. 4. Singularity point detection by dimension measurement

3. FEATURE ANALYSIS ON DEFECTIVE AREA

As we try to identify defects at the level of several micrometers through image processing as in our application, the presence of dust and foreign particles, though do not affect the quality of the final product, can have a critical effect on the production efficiency. Even if the manufacturing process is conducted in a clean environment of below class 1,000, it is almost impossible to eliminate all unwanted micrometer-ordered particles. Fig. 5 shows the defective images that have been identified in the inspection system and sent to the server for verification. In the inspection system, since all distinct points along the circuits are detected, we pick out not only real pattern defects but also foreign particles among the images.

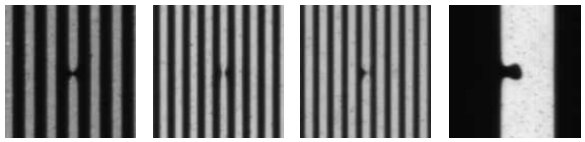

(a) Under-etching defects

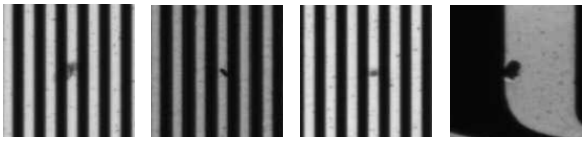

(b) Blemishes by foreign materials (Non defect)

Fig. 5. Typical defective images

When the process, materials, or environment is not controlled in the right way, and thereafter the products are exposed to the more unwanted foreign substances or particles, the more images due to blemishes are needed to be reviewed and judged by operators. To reduce unnecessary effort in verification and increase the efficiency of the system, these non defect blemishes need to be filtered before verification. As a mean to improve the efficiency for the inspection process, we came up with a statistic model based on the image features to discriminate and filter out the blemishes from the defective images. Fortunately, there are two noticeable differences between them and can be discriminated as a defective or a proper unit. Since most of the pattern defects related to short and protrusion are caused by unexpected local under-etching, they are represented by common, inherent features in shape: under etching produces a fluent curves along the pattern edge. On the other hand, blemishes due to particle adhesion are arbitrary shaped and produce abrupt edge changes around the pattern boundary. The second difference is on the view point of brightness of the defective area: protrusion or short is also a part of pattern and bears the same intensity as on the normal pattern, whereas particles tends to have high permeability to the light and are imaged brighter than the circuit region. Fig 6 depicts the overall procedure of the image analysis for feature extraction. The first step is segmentation of the defective region, a protrusion or a short, from an image for analysis. The segmentation is carried out by subtracting the reference image from the defective one, where the reference image is obtained through self-generation process based on fast-Fourier transform (FFT) technique. In this work, we consider only the defective images that are found in the straight patterned area for simplicity. Through the frequency domain analysis by FFT, the outline features of the pattern can be identified. In case of a straight pattern, the main component is placed along the pattern's orientation axis. Therefore, as we cut off the off-axis component in the frequency domain and perform inverse of the filtered FFT, a defect free image is revealed.

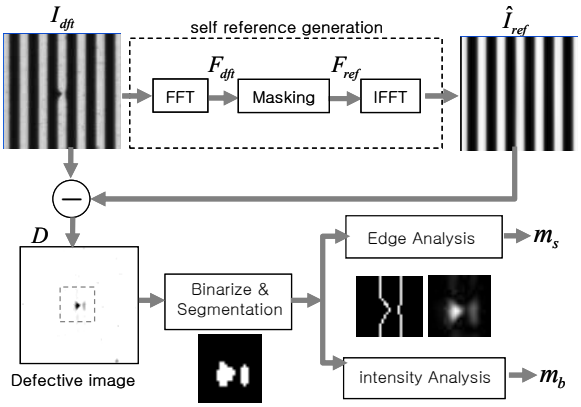

Fig 6. Image analysis for assessment index

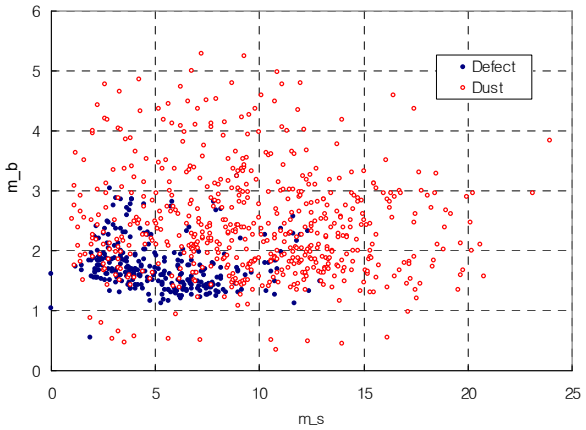

Fig.7. Defects and dust distribution in feature domain

To evaluate the pattern features and discriminate defects from blemishes, we define an index m_s that indicates the smoothness of variation in the edge orientation along the boundary.

$$m_s = \frac{1}{N}\sum_{i}^{N}\left|\delta\theta_i\right|, \tag{2}$$

Here, $\delta\theta_t$ is the orientation difference between the adjacent edge points. The orientation of an edge point is computed using Sobel operator as: (Davis)

$$\theta_i = tan^{-1}(g_y / g_x)_i \tag{3}$$

$$g_y = I_i \otimes S_y,\ g_x = I_i \otimes S_y,$$

$$S_x = \begin{bmatrix} -1 & 0 & 1 \\ -2 & 0 & 2 \\ -1 & 0 & 1 \end{bmatrix},\ S_y = \begin{bmatrix} 1 & 2 & 1 \\ 0 & 0 & 0 \\ -1 & -2 & -1 \end{bmatrix}.$$

To evaluate the brightness in the defective region, we define another index m_b that indicates the discrepancy of the intensity for the specific region compared to that of the pattern.

$$m_b = \frac{I_d}{I_p} \tag{4}$$

,where I_d and I_p are the average of the defective and pattern area, respectively.

To achieve a statistical model of the defect classifier we collected the indices, m_s and m_b, on test samples U (total 859 images), among which 571 blemish and 288 defect images are included. Fig. 7 shows a plot of the measured data in two dimensional spaces, where we can observe that the samples in the defect group G_{Dft} are distributed in a limited local area, whereas the samples belonging to the dust group G_{Dust} are scattered over a wide range.

4. BAYESIAN BASED CLASSIFICATION

4.1 Bayesian model.

Bayesian inference is a statistical data fusion algorithm based on Bayes' theorem of a posteriori probability to estimate a measure X with the pre-knowledge or the observation Z (Luo and Su, 1999) (Clark, and Yuille, 1990). Bayes' theorem provides the posterior conditional distribution of X=x, given Z=z, as

$$P(X = x \mid Z = z) = \frac{P(Z = z \mid X = x) \times P(X = x)}{P(Z = z)}. \tag{5}$$

When two observation z_1 and z_2 are available for the inference of a state x, and they are independence, the equation (3) can be extended as (Kumar *et al*., 2006):

$$P(x \mid Z = z_1, z_2) = \frac{P(Z = z_1, z_2 \mid x) \times P(x)}{P(Z = z_1, z_2)}. \tag{6}$$

The numerators and denominator could be achieved through the past observation, which describe the sensor model. A sensor output containing uncertainties is usually modeled as a mean about a true value with a variance. And Gaussian

distribution is frequently used to describe the sensor uncertainties, which is given by

$$P(Z=z \mid X=x)=\frac{1}{\sigma\sqrt{2\pi}}e^{\frac{-(x-z)^2}{2\sigma^2}} \quad . \qquad (7)$$

To incorporate the Bayesian inference model in our applications, the state and the sensory observations become $X=Dft$ and $Z=m_s,m_b$, respectively, and the inference model (6) is rewritten as equation (8). Here, we assume that the observations m_s and m_b on defective images are independent for simplicity.

$$P(Dft \mid m_s, m_b)=\frac{P(m_s \mid Dft)\times P(m_b \mid Dft)\times P(Dft)}{P(m_s, m_b)} \qquad (8)$$

Equation (8) implies a probability that a defect candidate image, of which the measures are observed as m_s and m_b, is a real defective one. A priori information about $P(m_s|Dft)$, $P(m_b|Dft)$, $P(Dft)$, and $P(m_b,m_s)$ are obtained from the collected test data in the previous chapter. Since the probability $P(Dft)$ is the defect ratio among the defect candidates, it is regarded here as constant 0.335 (=288/859). The distributions of the measures of defect images, $P(m_s|Dft)$ and $P(m_b|Dft)$, in feature domain are formulated here by using Gaussian functions for simplicity. Since the denominator term $P(m_b,m_s)$ is described with two observations, it is modeled by a two-dimensional joint Gaussian function which is given by

$$P(m_s, m_b)=\frac{1}{2\pi\sigma_s\sigma_b}e^{\frac{-(m_s-\bar{m}_s)^2}{2\sigma_s}+\frac{-(m_b-\bar{m}_b)^2}{2\sigma_b}} \quad . \qquad (9)$$

The parameters of the Gaussian probability models, the mean and variance, are computed from the collected measures in the previous chapter, which are listed in table 1. Fig. 8 illustrates the final probability density function of the Bayesian inference model according to the measures m_s and m_b.

Table 1. the parameters of the sensor model

	Mean	Variance
$P(m_s\|Dft)$	$\underline{m}_{s,Dft}$ = 5.239	$\sigma_{s,Dft}$= 2.592
$P(m_b\|Dft)$	$\underline{m}_{b,Dft}$ = 1.755	$\sigma_{b,Dft}$ = 0.413
$P(m_b,m_s)$	$\underline{m}_s$ = 8.203	σ_s= 4.545
	$\underline{m}_b$ = 2.207	σ_{bt} = 0.823

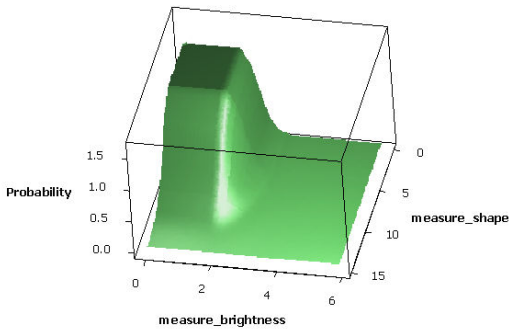

Fig. 8. Bayesian Probability model

We tested the Bayesian classifier on another image set of 2,083 defect candidate images, where 274 real defects are included. For the classification, we regard a defective image as a real defect when the probability output by the Bayesian model is larger than the threshold we set. The threshold, here, means the upper limit of the probability that a defect candidate is allowed to be filtered out as a dust image. Table 2 and Fig. 11 depict the test result.

Table 2. Experimental results on 2,083 images

	Defect images (274 images)		Dust images (1809 images)	
Threshold(%)	filtered units	overkill rate	filtered units	filtering rate
0.08	0	0.0	678	37.5
0.10	2	0.7	688	38.0
0.50	4	1.5	860	47.5
1.00	8	2.9	954	52.7
1.50	10	3.6	1015	56.1
2.00	11	4.0	1058	58.5
2.50	15	5.5	1095	60.5
3.00	17	6.2	1122	62.0
3.50	17	6.2	1142	63.1
4.00	21	7.7	1160	64.1
5.00	24	8.8	1172	64.8
6.00	26	9.5	1189	65.7
7.00	29	10.6	1200	66.3
8.00	30	10.9	1212	67.0
9.00	37	13.5	1227	67.8
10.00	39	14.2	1242	68.7
11.00	44	16.1	1256	69.4
12.00	46	16.8	1266	70.0
13.00	51	18.6	1273	70.4

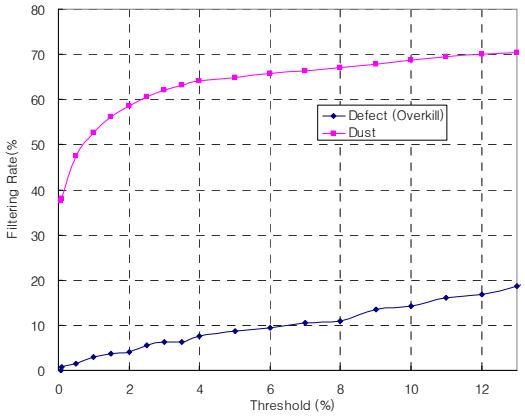

Fig. 9. Filtering and overkill rate according to threshold

As we increase the threshold, more and more dust images are filtered out, while a part of the real defects also are misclassified into dust ones. The performance of the classifier can be evaluated by the filtering rate for dust images, and the failure rate for real defects identification. The undesirable misclassification of real defects is considered here as failure, and is evaluated as over-kill rate. From the graph, as we place the priority on minimizing the over-kill rate along with a meaningful filtering rate, a threshold can be decided a value within 0.5% for this case.

Fig. 10 shows the over killed defects with a probability threshold of 0.5%, where we can find several exceptional cases in the defective areas: small particles or substance materials in nearby areas produce erroneous results. On the other hand, some dust bears such similar features to defects that they are hard to be discriminated and filtered out.

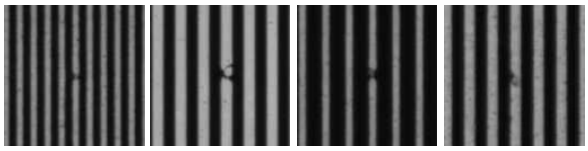

(a) over-killed images (real defects)

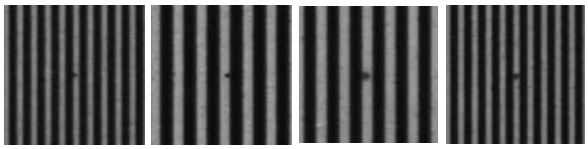

(b) under-killed images (dust)

Fig. 10. Mis-classified images with threshold 0.5

5. CONCLUSIONS

In this research we reported on increasing the efficiency of the TS inspection system by filtering unwanted trivial blemishes caused by dust or foreign substances. Three main achievements were made through this research. Firstly, we proposed a defective region segmentation algorithm by utilizing a self-generated reference image, which made it possible to extract image features of the local area in a reliable way. Secondly, the defined indices indicating the properties of under-etching defects gave us good clues to whether the defective image contains a pattern defect or a blemish by dust. Finally, the Bayesian inference model was successfully implemented for the classification of the defects and dust based on the image features. The experimental studies validated the proposed method: we could filter out about 47% of the defect candidate caused by dust, trivial blemishes which otherwise would have been singled out to be verified by operators, while limiting the overkill rate to below 0.15%. For future works, an investigation on another image feature to increase the classification accuracy will be conducted. And the proposed method, which is at this point confined to straight pattern areas, needs to be extended to general pattern areas.

REFERENCES

Bayes, T. (1763). *An Essay Towards Solving a Problem in Doctrine of Chances*, Philosophical Transactions, vol. 53, pp. 370-418.

Clark, J.J. and Yuille, A.L.(1990). *Data Fusion for Sensory Information Processing Systems*, Kluwer Academic Publications.

Davies, R. *Machine Vision,* Academic Press, San Diego, CA, USA,

Kumar, M., Garg, D.P. and Zachery, R.A.(2006). *A Generalized Approach for Inconsistency Detection in Data Fusion from Multiple Sensors*, Proc. Of American Control Conference, Minneapolis, USA, June, pp. 2078-2083.

Lim, D.C., Yang, H.G., Seo, D.G., and Jeong, D.H. (2004). *Real-Time Defect Classification for the inspection of TFT Glass*, Vision Engineering Workshop 2004, Yokohama, Japan, pp. 81-85.

Lim, D.C., Yun, S.Y., Jung B.Y., and Hong, C.K.(2001). *Optical Inspection Method of Lead Frame using Mathematical Morphology,* Proc. Of SPIE, Optomechatronic Systems II, pp. 107-114.

Luo, R. and Su, K. (1999). *A Review of High-Level Multisensor Fusion: Approaches and Applications*, Proc. of the IEEE International Conference on Multisensor Fusion and Integration for Intelligent Systems, pp. 25-31.

Moganti M., and Ercal, F.(1995). *Automatic PCB Inspection Systems,* IEEE Potentials, **vol. 14**, no. 3, pp. 6-10.

Moganti, M., Ercal, F., Dagli, C.H., Tsunekawa, S.(1996). *Automatic PCB Inspection Algorithms: A survey*, Computer Vision and Image Understanding, **vol. 63**, No. 2, pp. 287-313.

Thompson, T., Carrasco, A., and Mawer, A.(1999) *Reliability assessment of a thin(flex) BGA using a polymide tape substrate,* Electronics Manufacturing Technology Symposium, Austin, TX, pp. 207-213.

Roh, Y.J., Kim, C.W., Lee, H.H., and Jeong, D.H. (2005). *Tile-Matching Based Image Correction of a High Resolution Image for Tape Substrate (TS) Inspection*, Proceedings of Vision Engineering Workshop, pp. 279-285.

Roh, Y.J., Shin, H.S., Kim, C.W.,Lee, H.H. Lee, and Jeong, D.H.(2006). *A Boundary Tracking Approach for Tape Substrate Pattern Inspection Based on Skeleton Information*, Proc. of SPIE, **vol. 6375**, Optomechatronic Sensors, Instrumentation, and Computer-vision Systems, pp. 6375P1-6375P11.